ORGANOMETALLICS

Article

pubs.acs.org/Organometallics

Synthesis and Reactivity of Four- and Five-Coordinate Low-Spin Cobalt(II) PCP Pincer Complexes and Some Nickel(II) Analogues

Sathiyamoorthy Murugesan,[†] Berthold Stöger,[‡] Maria Deus Carvalho,[§] Liliana P. Ferreira,[∥,⊥] Ernst Pittenauer,[‡] Günter Allmaier,[‡] Luis F. Veiros,[#] and Karl Kirchner*[,†]

[†]Institute of Applied Synthetic Chemistry and [‡]Institute of Chemical Technologies and Analytics, Vienna University of Technology, Getreidemarkt 9, A-1060 Vienna, Austria

[§]Centro de Química e Bioquímica/DQB and [∥]Centro de Física da Matéria Condensada, Faculdade de Ciências, Universidade de Lisboa, 1749-016 Lisboa, Portugal

[⊥]Department of Physics, University of Coimbra, 3004-516 Coimbra, Portugal

[#]Centro de Química Estrutural, Instituto Superior Técnico, Universidade de Lisboa, Avenida Rovisco Pais No. 1, 1049-001 Lisboa, Portugal

Supporting Information

ABSTRACT: Anhydrous $CoCl_2$ or $[NiCl_2(DME)]$ reacts with the ligand PCP^{Me}-*i*Pr (**1**) in the presence of *n*BuLi to afford the 15*e* and 16*e* square planar complexes $[Co(PCP^{Me}$-*i*Pr)Cl] (**2**) and $[Ni(PCP^{Me}$-*i*Pr)Cl] (**3**), respectively. Complex **2** is a paramagnetic d^7 low-spin complex, which is a useful precursor for a series of Co(I), Co(II), and Co(III) PCP complexes. Complex **2** reacts readily with CO and pyridine to afford the five-coordinate square-pyramidal 17*e* complexes $[Co(PCP^{Me}$-*i*Pr)(CO)Cl] (**4**) and $[Co(PCP^{Me}$-*i*Pr)(py)Cl] (**5**), respectively, while in the presence of Ag^+ and CO the cationic complex $[Co(PCP^{Me}$-*i*Pr)$(CO)_2]^+$ (**6**) is afforded. The effective magnetic moments μ_{eff} of all Co(II) complexes were derived from the temperature dependence of the inverse molar magnetic susceptibility by SQUID measurements and are in the range 1.9 to 2.4 μ_B. This is consistent with a d^7 low-spin configuration with some degree of spin−orbit coupling. Oxidation of **2** with $CuCl_2$ affords the paramagnetic Co(III) PCP complex $[Co(PCP^{Me}$-*i*Pr)$Cl_2]$ (**7**), while the synthesis of the diamagnetic Co(I) complex $[Co(PCP^{Me}$-*i*Pr)$(CO)_2]$ (**8**) was achieved by stirring **2** in toluene with KC_8 in the presence of CO. Finally, the cationic 16*e* Ni(II) PCP complex $[Ni(PCP^{Me}$-*i*Pr)(CO)$]^+$ (**10**) was obtained by reacting complex **3** with 1 equiv of $AgSbF_6$ in the presence of CO. The reactivity of CO addition to Co(I), Co(II), and Ni(II) PCP square planar complexes of the type $[M(PCP^{Me}$-*i*Pr)(CO)$]^n$ (n = +1, 0) was investigated by DFT calculations, showing that formation of the Co species, **6** and **8**, is thermodynamically favorable, while Ni(II) maintains the 16*e* configuration since CO addition is unfavorable in this case. X-ray structures of most complexes are provided and discussed. A structural feature of interest is that the apical CO ligand in **4** deviates significantly from linearity, with a Co−C−O angle of 170.0(1)°. The DFT-calculated value is 172°, clearly showing that this is not a packing but an electronic effect.

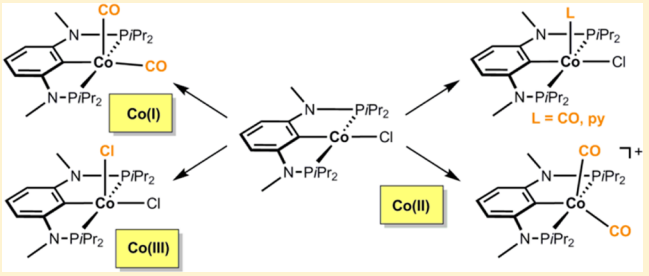

INTRODUCTION

One of the ways of modifying and controlling the properties of transition metal complexes is the use of appropriate ligand systems such as pincer ligands, i.e., tridentate ligands that are coordinated in meridional fashion. Usually consisting of a central aromatic backbone tethered to two two-electron donor groups by different spacers, this class of tridentate ligands has found numerous applications in various areas of chemistry, including catalysis, due to their combination of stability, activity, and variability.[1] We are currently focusing on the synthesis and reactivity of transition metal PNP and PCP pincer complexes where the pincer ligands contain amine (NH and NR) linkers between the aromatic ring and the phosphine moieties.[2] These types of PNP and PCP ligands are readily available via condensation reactions between various 2,6-diaminopyridines and 1,3-diaminobenzenes and electrophilic chlorophosphines R_2PCl. These ligands can be designed in modular fashion and are thus very versatile ligand platforms. This has resulted in the preparation of a series of square planar group 10 metal PCP complexes,[3] as well as numerous iron[4] and molybdenum PNP systems.[5]

Currently we are focusing on the chemistry of nonprecious metal PCP pincer complexes in particular with the metals cobalt, nickel, and molybdenum. Surprisingly, as cobalt is concerned only a few PCP pincer complexes featuring a direct cobalt−carbon single bond have been reported in the literature. An overview of cobalt PCP pincer systems (**A**−**E**), mostly

Received: July 30, 2014
Published: October 9, 2014

   dx.doi.org/10.1021/om5007769 | *Organometallics* 2014, 33, 6132−6140

based on the Co(I)/Co(III) oxidation states, is depicted in Scheme 1.[6−10] It has to be noted that several related cobalt complexes containing anionic pincer-type PNP, PSiP, NCN, and NNN frameworks are described.[11−19]

Scheme 1. Overview of Co PCP Complexes Reported in the Literature

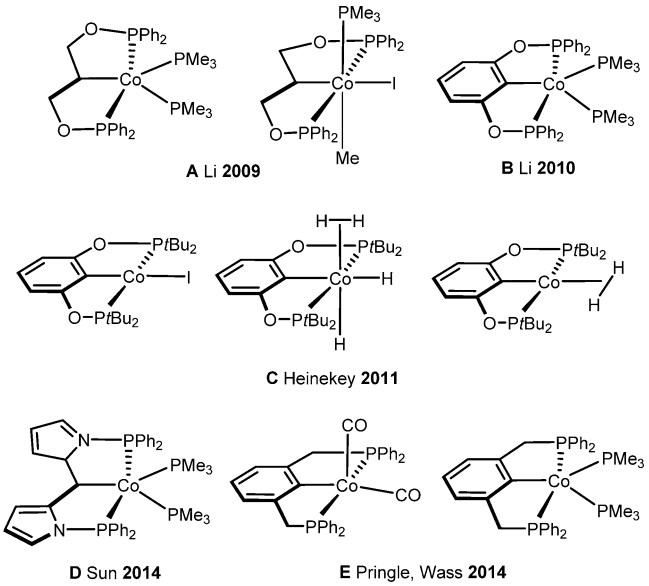

Here we report on the synthesis, characterization, and reactivity of a series of new cobalt PCP pincer complexes in oxidation states +I, +II, and +III based on the d^7 low-spin Co(II) complex [Co(PCP^{Me}-*i*Pr)Cl] where the P*i*Pr$_2$ moieties of the PCP ligand are connected to the benzene ring via NMe linkers. For comparison, the syntheses of some analogous low-spin d^8 Ni(II) PCP complexes are also reported.

RESULTS AND DISCUSSION

Treatment of anhydrous $CoCl_2$ or [$NiCl_2$(DME)] (DME = 1,2-dimethoxyethane) with the ligand PCP^{Me}-*i*Pr (**1**) in the presence of *n*BuLi in THF affords the 15*e* and 16*e* complexes [Co(PCP^{Me}-*i*Pr)Cl] (**2**) and [Ni(PCP^{Me}-*i*Pr)Cl] (**3**) in 96% and 97% isolated yields, respectively (Scheme 2). The Co(II)

Scheme 2. Synthesis of Complexes [Co(PCP^{Me}-*i*Pr)Cl] (2) and [Ni(PCP^{Me}-*i*Pr)Cl] (3)

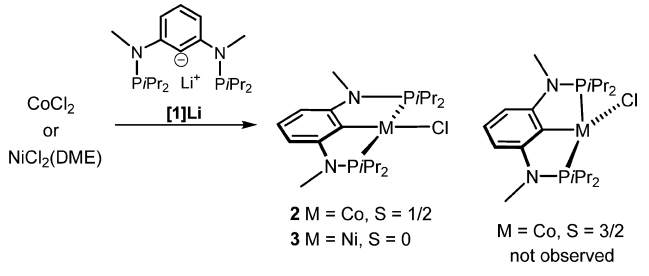

complex displays large paramagnetic shifted and very broad ^{1}H NMR signals, which were thus not very informative. $^{13}C\{^1H\}$ and $^{31}P\{^1H\}$ NMR could not be detected at all. The magnetic moment of μ_{eff} = 2.3(1) μ_B was derived from the temperature dependence of the inverse molar magnetic susceptibility, which is well described by a Curie law above 10 K (one unpaired electron). This value is higher than the one expected for the spin-only approximation and is explained by a spin−orbit coupling contribution, being consistent with a low-spin square planar complex.[20] DFT calculations[21] reveal that the corresponding high-spin Co(II) complex with S = 3/2, which adopts a pseudotetrahedral geometry, is 19.5 kcal/mol less stable[22] than the square planar low-spin state with S = 1/2 and was not observed experimentally (Figure 1). Solution equilibria

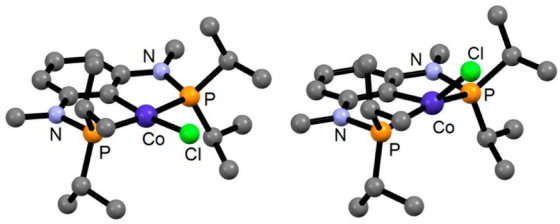

Figure 1. Optimized B3LYP geometries of the low-spin (left) and high-spin (right) isomers [Co(PCP^{Me}-*i*Pr)Cl] (**2**). Hydrogen atoms are omitted for clarity.

between square planar low-spin and tetrahedral high-spin species, which are also accompanied by color changes, were observed for the related Co(II) pincer-type complexes [Co(PNP)Cl], where PNP are anionic disilylamido PNP ligands [$N(SiMe_2CH_2PPh_2)_2$]$^-$ and [N-($SiMe_2CH_2PtBu_2$)$_2$]$^-$.[11,12d] The Ni(II) complex, as expected, is diamagnetic and was fully characterized by NMR spectroscopy and elemental analysis.

The solid-state structures of these complexes were determined by X-ray diffraction, and representations of the molecules are presented in Figures 2 and 3. Selected metrical

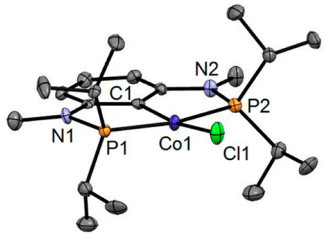

Figure 2. Structural view of [Co(PCP^{Me}-*i*Pr)Cl] (**2**) showing 50% thermal ellipsoids (H atoms and a second independent complex are omitted for clarity).

parameters for **2** and **3** are given in Table 1 and in the figure captions, respectively. It has to be noted that structurally

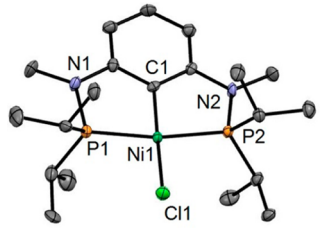

Figure 3. Structural view of [Ni(PCP^{Me}-*i*Pr)Cl] (**3**) showing 50% thermal ellipsoids (H atoms and three other independent complexes are omitted for clarity). Selected bond lengths (Å) and bond angles (deg): Ni1−P1 2.1811(5), Ni1−P2 2.1800(5), Ni1−C1 1.915(2), Ni1−Cl1 1.785(2), P1−Ni1−P2 165.79(2), C1−Ni1−Cl1 175.30(7).

dx.doi.org/10.1021/om5007769 | *Organometallics* 2014, 33, 6132−6140

Table 1. Selected Bond Distances (Å) and Angles (deg) for the Co(II) PCP Complexes [Co(PCP^{Me}-*i*Pr)Cl] (2), [Co(PCP^{Me}-*i*Pr)(CO)Cl] (4), [Co(PCP^{Me}-*i*Pr)(py)Cl] (5), and [Co(PCP^{Me}-*i*Pr)(CO)$_2$]SbF$_6$ (6)

	2	4	5	6
Co1−C1	1.919(2)	1.950(1)	1.946(1)	1.953(2)
Co1−P1	2.192(1)	2.2066(4)	2.2206(3)	2.2270(6)
Co1−P2	2.184(1)	2.2134(4)	2.2057(4)	2.2154(6)
Co1−Cl1	2.234(1)	2.2743(4)	2.3103(4)	
Co1−C21		1.800(1)		1.821(2)
Co1−C22				1.833(2)
Co1−N3			2.1417(8)	
P1−Co1−P2	167.00(3)	159.06(1)	158.44(1)	162.32(2)
C1−Co1−Cl1	171.40(9)	151.49(3)	166.89(3)	
Co1−C21−O1		170.0(1)		176.6(3)
Co1−C22−O2				176.7(2)
C1−Co1−N3			96.28(3)	
C1−Co1−C21				143.62(8)
C1−Co1−C22				123.0(1)
C21−Co1−C22				93.3(1)

characterized square planar complexes of Co(II)-Cl are rare, generally requiring strong-field ligands.[12e] The molecular structures of all these compounds show the metal in a typical slightly distorted square planar conformation with the PCP ligands coordinated to the metal center in a tridentate meridional mode. In both complexes the C1−Co−Cl1 angles deviate slightly from linearity, being 171.40(9)° and 175.30(7)°, respectively. The P(1)−Co−P2 angles are 167.00(3)° and 159.06(1)°, respectively.

Complex **2** reacts readily with the simple ligands CO and pyridine to afford the five-coordinate square-pyramidal 17*e* complexes [Co(PCP^{Me}-*i*Pr)(CO)Cl] (**4**) and [Co(PCP^{Me}-*i*Pr)(py)Cl] (**5**) in 94% and 95% isolated yields, respectively (Scheme 3). These complexes are paramagnetic, and ^{1}H NMR spectra gave rise to broad and featureless signals and were not very informative. ^{13}C{^{1}H} and ^{31}P{^{1}H} NMR signals could again not be detected at all. The magnetic properties of **4** and **5** were studied by SQUID magnetometry. The cobalt effective magnetic moments extracted from a Curie law fitting to inverse molar susceptibility data were 2.0(1) and 2.4(1) μ_B, respectively, consistent with a low-spin d^7 center (one unpaired electron), again with some degree of second-order spin−orbit coupling. Moreover, the CO ligand in **4** gives rise to a strong absorption at 1948 cm^{-1}, indicating strong π-back-bonding from the metal center (cf. 2143 cm^{-1} in free CO). This is also in accordance with the fact that the CO ligand is not removable under vacuum at 25 °C within several days. Complex **3**, on the other hand, does not react with CO or pyridine to give five-coordinate 18*e* complexes but maintains its square planar geometry.

The solid-state structures of **4** and **5** were determined by single-crystal X-ray diffraction. Structural diagrams are depicted in Figures 4 and 5 with selected bond distances given in Table 1. Both complexes exhibit a distorted square pyramidal coordination with CO and py in the apical position. The C−Co−Cl angles of **4** and **5** are 151.49(3)° and 166.89(3)°, respectively, thus strongly deviating from linearity. The P−Co−P angles are 159.06(1)° and 158.44(1)°, respectively. A structural feature of interest is that the apical CO ligand in **4** deviates significantly from linearity with a Co−C−O angle of 170.0(1)°. The DFT-calculated value is 172°, clearly showing

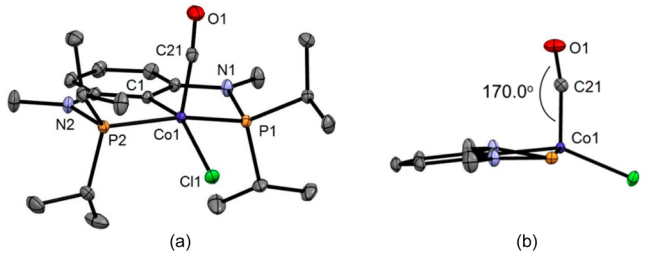

Figure 4. (a) Structural view of [Co(PCP^{Me}-*i*Pr)(CO)Cl] (**4**) showing 50% thermal ellipsoids (H atoms omitted for clarity). (b) Inner part of **4** showing the square pyramidal structure as well as the significant bending of the apical CO ligand.

Scheme 3. Synthesis of Co(I), Co(II), and Co(III) PCP Complexes Based on [Co(PCP^{Me}-*i*Pr)Cl] (2)

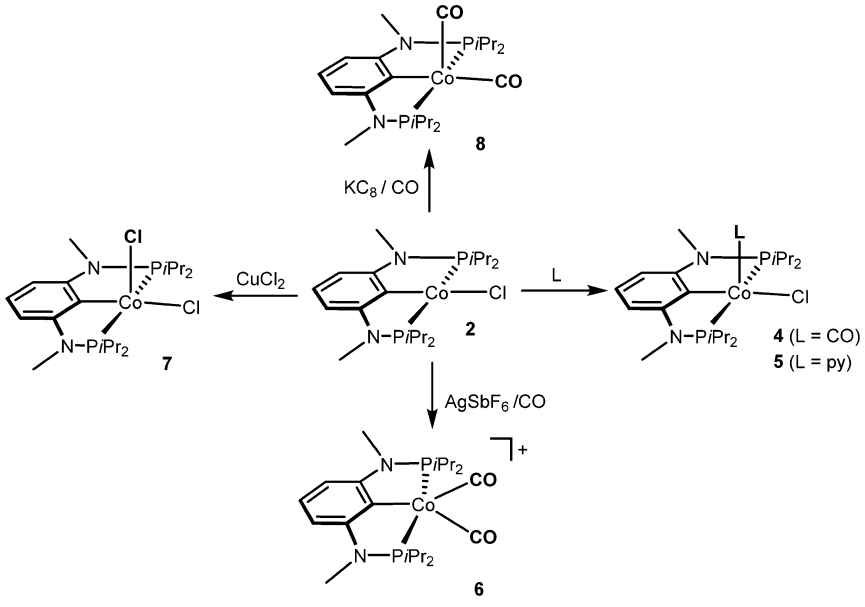

dx.doi.org/10.1021/om5007769 | *Organometallics* 2014, 33, 6132−6140

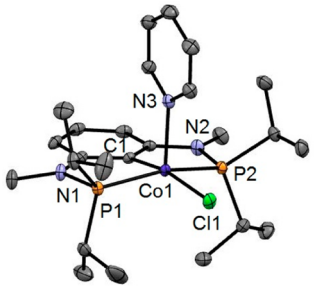

Figure 5. Structural view of [Co(PCP^{Me}-*i*Pr)(py)Cl] (**5**) showing 50% thermal ellipsoids (H atoms are omitted for clarity).

that this is not a packing but an electronic effect. Similar structural peculiarities have been observed for square pyramidal Fe(0) complexes of the type [Fe(PNP-*t*Bu)(CO)$_2$] (PNP = N,N′-bis(di-*tert*-butylphosphinomethyl)pyridine), where this issue has been discussed in detail.[23] The bending of the apical CO ligand in **4** may also be rationalized by the theoretical investigations of Hoffmann on five-coordinate metal nitrosyl complexes.[24]

The electronic structures of complexes **2** and **4** were evaluated by DFT calculations. Representations of the frontier molecular orbitals and spin density plots are presented in Figure 6. The electronic structures correspond to low-spin Co(II) complexes with the SOMO centered in the d_{z^2} orbital of the metal. The spin density plots confirm this view of the electronic structure with practically all the unpaired spin located on the cobalt center. There is an important participation of the PCP ligand in the second occupied molecular orbital of each complex, but no significant unpaired spin density is observed in the ligands.

Under a CO atmosphere in the presence of 1 equiv of $AgSbF_6$, complex **2** reacts readily to give the cationic dicarbonyl complex [Co(PCP^{Me}-*i*Pr)(CO)$_2$]$^+$ (**6**) in 93% yield (Scheme 3). This complex exhibits an effective magnetic moment of 1.9(1) μ_B in agreement with a d^7 low-spin electron configuration. Complex **6** exhibits two bands at 2013 and 2046 cm^{-1} in the IR spectrum for the mutually *cis* CO ligands assignable to the symmetric and asymmetric CO stretching frequencies, respectively.

Moreover, complex **6** was also investigated by means of ESI-MS in the positive ion mode in a CH_3CN solution. Under so-called "soft ionization" conditions, only one signal was observed at *m*/*z* 454.2, which corresponds to the mono CO fragment [Co(PCP^{Me}-*i*Pr)(CO)]$^+$ ([M − CO]$^+$). This clearly suggests that one CO ligand in **6** is labile. An X-ray structure of **6** is shown in Figure 7, with selected bond distances and angles provided in Table 1. In contrast to complexes **4** and **5**, the overall geometry of **6** about the cobalt center is better described as distorted trigonal bipyramidal. The two carbonyl ligands and the benzene carbon C1 define the equatorial plane with bond angles of 93.3(1)°, 143.6(1)°, and 123.0(1)° for C21−Co1−C22, C1−Co1−C21, and C1−Co1−C22, respectively. A

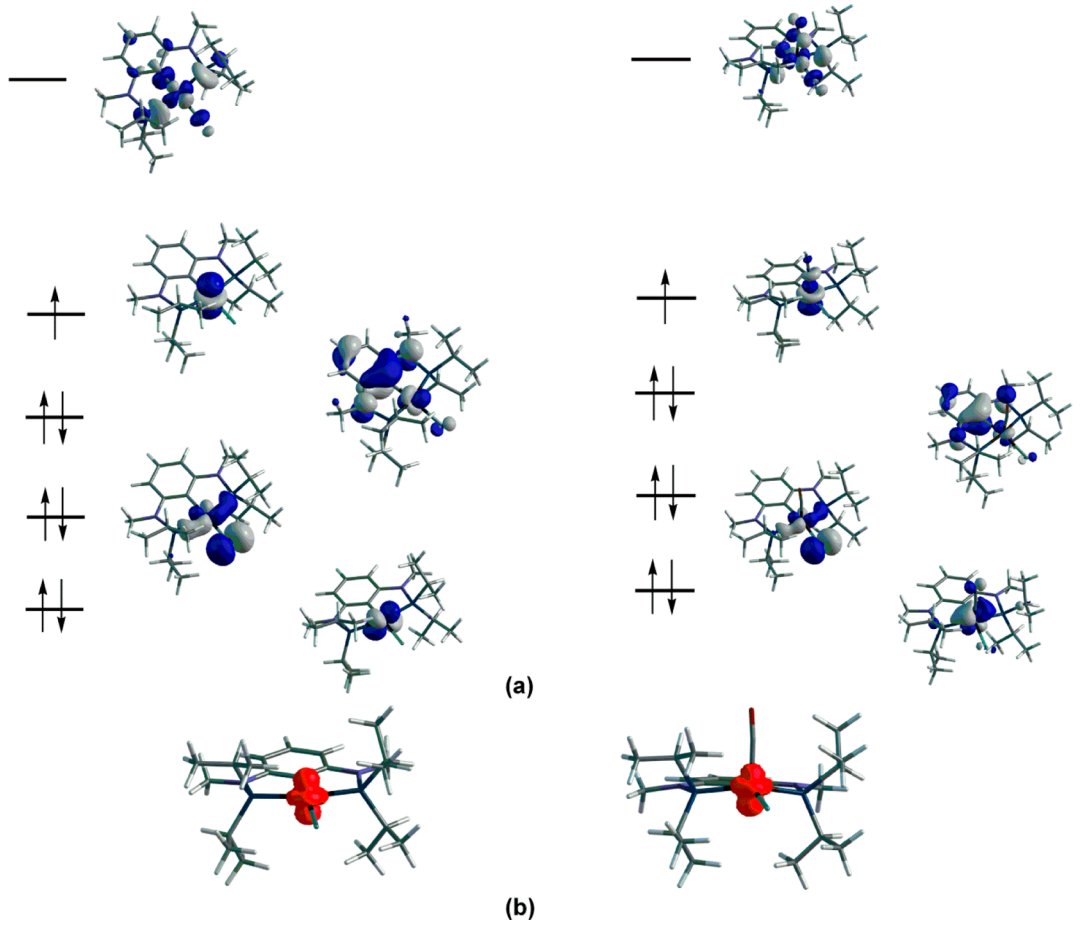

Figure 6. (a) DFT-computed frontier orbitals (d-splitting) and (b) spin density for [Co(PCP^{Me}-*i*Pr)Cl] (**2**) (left) and for [Co(PCP^{Me}-*i*Pr)(CO)Cl] (**4**) (right).

dx.doi.org/10.1021/om5007769 | *Organometallics* 2014, 33, 6132−6140

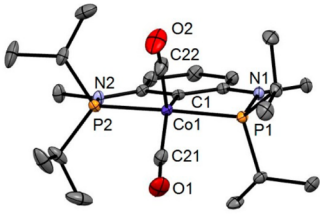

Figure 7. Structural view of $[Co(PCP^{Me}\text{-}iPr)(CO)_2]SbF_6$ (**6**) showing 50% thermal ellipsoids (H atoms and SbF_6^- counterion are omitted for clarity).

significant distortion is also observed in the axial phosphine ligands, where the P1−Co1−P2 bond angle of 162.32(2)° is contracted toward the benzene ring. The CO ligands exhibit some bending with Co1−C21−O1 and Co1−C22−O2 angles of 176.6(3)° and 176.7(2)°, respectively, and is thus not as pronounced as in complex **4**, where the Co1−C21−O1 angle is only 170.0(1)°.

The metal−ligand bond lengths are generally sensitive to spin state. With respect to low-spin Co(II), a typical Co(II)−C(sp^2) bond distance is 1.994(3) Å, as in the low-spin square planar cobalt(II) aryl complex $[Co(PEt_2Ph)_2(mesityl)_2]$.[25] In complexes **2**, **4**, **5**, and **6** the Co−C(sp^2) distances are in the range 1.919 to 1.953 Å. Typical low-spin Co(II)−P bond distances are 2.2127(8) and 2.2162(8) Å such as in $[Co(CH_2Ph)\{N(SiMe_2CH_2PPh_2)_2\}]$.[11] The Co(II)−P bond distances of complexes **2**, **4**, **5**, and **6** are in range 2.184 to 2.227 Å. Accordingly, both Co−C and Co−P bond distances are fully consistent with the low-spin nature of these complexes.

Oxidation of **2** with $CuCl_2$ cleanly affords the paramagnetic five-coordinate Co(III) PCP complex $[Co(PCP^{Me}\text{-}iPr)Cl_2]$ (**7**) in 93% isolated yield (Scheme 3). The solution magnetic moment of 3.1 μ_B (Evans method)[26] is consistent with a d^6 intermediate spin system, corresponding to two unpaired electrons, and is within the observed range of other five-coordinate Co(III) complexes known.[11] This complex displays a large paramagnetic shifted ^1H NMR spectrum. At room temperature the line widths are relatively narrow in this particular case, and thus, some ligand resonances could be assigned on the basis of integration. $^{13}C\{^1H\}$ and $^{31}P\{^1H\}$ NMR signals could not be detected at all. A structural view of this complex is shown in Figure 8, with selected bond distances and angles reported in the caption. The molecular structure shows the metal in a distorted square pyramidal conformation, which is not uncommon for five-coordinate Co(III) complexes.[11]

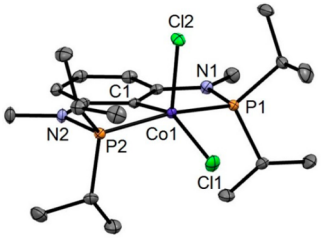

Figure 8. Structural view of $[Co(PCP^{Me}\text{-}iPr)Cl_2]$ (**7**) showing 50% thermal ellipsoids (H atoms are omitted for clarity). Selected bond lengths (Å) and bond angles (deg): Co1−P1 2.2549(4), Co1−P2 2.2602(4), Co1−C1 1.937(1), Co1−Cl1 2.2635(4), Co1−Cl2 2.2918(3), P1−Co1−P2 161.16(1), C1−Co1−Cl1 148.87(3), C1−Co1−Cl2 106.77(3), Cl1−Co1−Cl2 104.36(1).

Treatment of **7** with $AgSbF_6$ in CH_3CN affords, on workup, the diamagnetic tris-acetonitrile complex $[Co(PCP^{Me}\text{-}iPr)(CH_3CN)_3](SbF_6)_2$ (**9**) (Scheme 4). This complex was characterized by a combination of elemental analysis and ^1H, $^{13}C\{^1H\}$, and $^{31}P\{^1H\}$ NMR spectroscopy.

Scheme 4. Synthesis of $[Co(PCP^{Me}\text{-}iPr)(CH_3CN)_3]^{2+}$ (9)

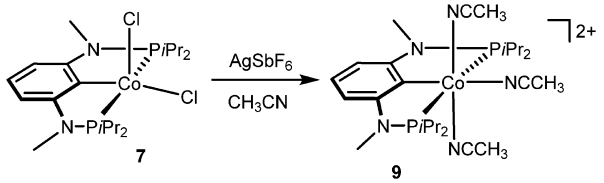

The synthesis of the Co(I) complex $[Co(PCP^{Me}\text{-}iPr)(CO)_2]$ (**8**) was achieved by stirring **2** in toluene with stoichiometric amounts of the strong reducing agent KC_8 in the presence of carbon monoxide (Scheme 3). This compound was obtained in 90% isolated yield as an air-sensitive but thermally stable yellow solid. The identity of this complex was unequivocally established by ^1H, $^{13}C\{^1H\}$, and $^{31}P\{^1H\}$ NMR, IR spectroscopy, and elemental analysis. Complex **8** exhibits two bands at 1906 and 1963 cm^{-1} in the IR spectrum for the mutually *cis* CO ligands assignable to the symmetric and asymmetric CO stretching frequencies, respectively. For comparison, the IR spectrum of the related Co(I) complex $[Co(PCP\text{-}Ph)(CO)_2]$[10] (PCP-Ph = 1,3-bis(diphenylphosphinomethyl)benzene) shows two bands, at 1929 and 1982 cm^{-1}, slightly shifted to higher wave numbers, indicating that PCP-*i*Pr is a stronger donor than PCP-Ph. In the cationic Co(II) complex $[Co(PCP^{Me}\text{-}iPr)(CO)_2]^+$ (**6**) these bands were found at 2013 and 2046 cm^{-1}. The shift of the CO bands to even higher wave numbers is consistent with the more electron-rich Co(I) center in **8**. In the $^{13}C\{^1H\}$ NMR spectrum the CO ligand gives rise to a low-field resonance as a poorly resolved triplet centered at 207.6 ppm. In the $^{31}P\{^1H\}$ NMR spectrum a singlet at 170.7 ppm is observed.

The molecular structure of **8** was determined by X-ray crystallography. A structural view is depicted in Figure 9, with

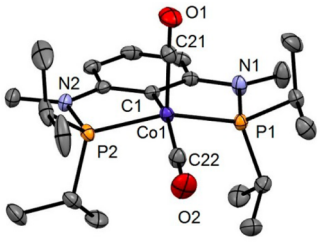

Figure 9. Structural view of $[Co(PCP^{Me}\text{-}iPr)(CO)_2]$ (**8**) showing 50% thermal ellipsoids (H atoms and a second independent complex are omitted for clarity). Selected bond lengths (Å) and bond angles (deg): Co1−P1 2.1710(5), Co1−P2 2.1740(5), Co1−C1 1.998(2), Co1−C21 1.799(2), Co1−C22 1.743(2), P1−Co1−P2 147.69(2), C1−Co1−C21 99.94(8), C1−Co1−C22 154.76(7), C21−Co1−C22 105.28(8), Co1−C21−O1 175.1(2), Co1−C22−O2 178.0(1).

selected bond distances and angles reported in the caption. This complex adopts basically a distorted square pyramidal geometry with C1−Co1−C21 and C1−Co1−C22 angles of 99.94(8)° and 154.76(7)°, respectively. The P1−Co1−P1 angle is comparatively small, being 147.69(2)° (cf 167.0°, 159.1°, 158.4°, and 162.3° in **2**, **4**, **5**, and **6**, respectively). In

dx.doi.org/10.1021/om5007769 | *Organometallics* 2014, 33, 6132−6140

Scheme 5. Synthesis of [Ni(PCP^{Me}-*i*Pr)(CO)]$^+$ (10)

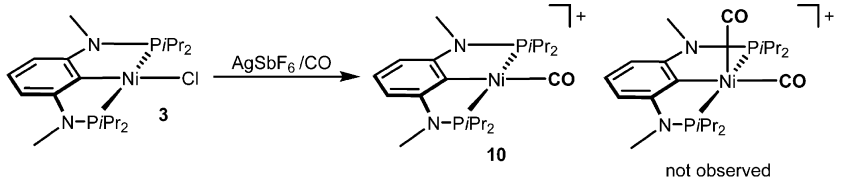

this case, in contrast to **4**, the CO ligands do not deviate significantly from linearity, with Co1−C21−O1 and Co1−C22−O2 angles of 178.0(1)° and 175.1(2)°, respectively. The structure of **8** is very different from the structure of the related complex [Co(PCP-Ph)(CO)$_2$],[10] which adopts a distorted trigonal bipyramidal geometry, with an unusually small P−Co−P angle of 134.6(1)°.

Finally, the cationic 16*e* Ni(II) PCP complex [Ni(PCP^{Me}-*i*Pr)(CO)]$^+$ (**10**) was obtained by reacting complex **3** with 1 equiv of AgSbF$_6$ in the presence of CO (Scheme 5). The formation of a dicarbonyl complex was not observed. Complex **10** is diamagnetic and has been characterized by a combination of ^{1}H, ^{13}C{^{1}H}, and ^{31}P{^{1}H} NMR, IR spectroscopy, and elemental analysis. In the IR spectrum an intense carbonyl band was observed at 2051 cm^{-1}. In the ^{13}C{^{1}H} NMR spectrum the CO ligand gives rise to a low-field resonance triplet centered at 189.9 ppm with a coupling constant J_{CP} of 13.7 Hz. A singlet at 148.6 ppm is observed in the ^{31}P{^{1}H} NMR spectrum. In the full scan ESI-MS of **10** in the positive ion mode in CH$_3$CN only signals at *m*/*z* 453.2 and 425.2 were detected, corresponding to the intact complex [Ni(PCP^{Me}-*i*Pr)(CO)]$^+$ (**10**) ([M]$^+$) and the fragment [Ni(PCP^{Me}-*i*Pr)]$^+$ ([M − CO]$^+$). This clearly shows that **10** is more labile than the corresponding cationic mono-CO fragment of Co(II), viz., [Co(PCP^{Me}-*i*Pr)(CO)]$^+$, where CO dissociation was not observed in the full-scan ESI-MS.

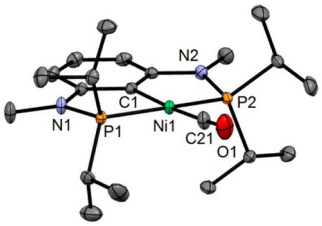

Figure 10. Structural view of [Ni(PCP^{Me}-*i*Pr)(CO)]SbF$_6$ (**10**) showing 50% thermal ellipsoids (H atoms, a second independent complex, and SbF$_6^-$ counterion are omitted for clarity). Selected bond lengths (Å) and bond angles (deg): Ni1−P1 2.1811(5), Ni1−P2 2.1800(5), Ni1−C1 1.915(2), Ni1−C21 1.785(2), P1−Ni1−P2 165.79(2), C1−Ni1−C21 175.30(7), Ni1−C21−O1 176.5(2).

The addition of CO to the 15*e* and 16*e* complexes [Co(PCP^{Me}-*i*Pr)(CO)]^n (*n* = +1, 0) and to [Ni(PCP^{Me}-*i*Pr)(CO)]$^+$ was also studied by means of DFT calculations, showing that the reaction is exergonic by −6.4 and by −9.3 kcal/mol for the cationic and the neutral Co complexes, respectively, while it is endergonic by 6.5 kcal/mol in the case of [Ni(PCP^{Me}-*i*Pr)(CO)]$^+$ (**10**) (Scheme 6).[27] This indicates that four-coordinate Co complexes are able to add a fifth ligand, forming either square pyramidal or trigonal bipyramidal complexes, while Ni(II) typically remains in the 16*e* configuration. This, of course, may also have significant implications in catalysis with respect to substrate binding and activation.

Scheme 6. Free Energies (kcal/mol) Calculated for the Addition of CO to the 15*e* and 16*e* Square Planar Complexes [Co(PCP^{Me}-*i*Pr)(CO)]^n (*n* = +1, 0) and [Ni(PCP^{Me}-*i*Pr)(CO)]$^+$

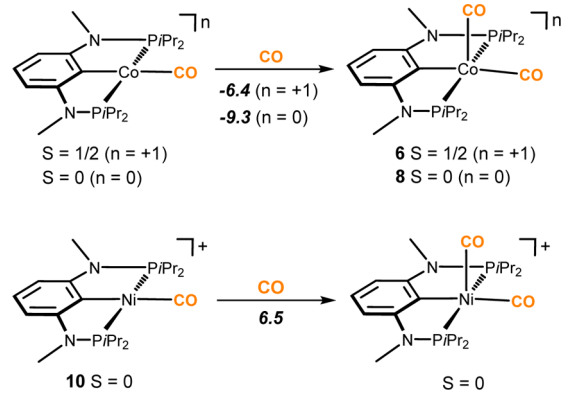

CONCLUSION

We have shown here that a PCP pincer ligand based on 1,3-diaminobenzene acts as versatile supporting scaffold in cobalt chemistry. The PCP moiety provides access to a range of Co complexes in formal oxidation states +I, +II, and +III by utilizing the 15*e* square planar d^7 complex [Co(PCP^{Me}-*i*Pr)Cl] (**2**) as synthetic precursor. In contrast to the analogous Ni(II) complex [Ni(PCP^{Me}-*i*Pr)Cl] (**3**), **2** is able to form stable pentacoordinate square pyramidal or trigonal bipyramidal 17*e* complexes. For instance, **2** readily adds CO and pyridine to afford the five-coordinate square pyramidal complexes [Co(PCP^{Me}-*i*Pr)(CO)Cl] (**4**) and [Co(PCP^{Me}-*i*Pr)(py)Cl] (**5**), respectively, while in the presence of Ag$^+$ and CO the cationic bipyramidal complex [Co(PCP^{Me}-*i*Pr)(CO)$_2$]$^+$ (**6**) is formed. The effective magnetic moments μ_{eff} of all Co(II) complexes derived from the temperature dependence of the inverse molar magnetic susceptibility by SQUID measurements are in the range 1.9 to 2.4 μ_B. This is consistent with a d^7 low-spin configuration with a contribution from the second-order spin−orbit coupling. Oxidation of **2** with CuCl$_2$ yields the Co(III) PCP complex [Co(PCP^{Me}-*i*Pr)Cl$_2$] (**7**), while the synthesis of the Co(I) complex [Co(PCP^{Me}-*i*Pr)(CO)$_2$] (**8**) was achieved by reducing **2** with KC$_8$ in the presence of CO. Complex **7** exhibits a solution magnetic moment of 3.1 μ_B, which is consistent with a d^6 intermediate spin system. The tendency of Co(I), Co(II), and Ni(II) PCP complexes of the type [M(PCP^{Me}-*i*Pr)(CO)]^n (*n* = +1, 0) to add CO was investigated by DFT calculations, showing that the Co species readily form the five-coordinate complexes **6** and **8**, which are thermodynamically favorable, while Ni(II) maintains the 16*e* configuration since CO addition is thermodynamically unfavorable in this case. X-ray structures of most complexes are provided and

dx.doi.org/10.1021/om5007769 | Organometallics 2014, 33, 6132−6140

discussed. A structural feature of interest is that the CO ligand in **4** deviates significantly from linearity with a Co−C−O angle of 170.0(1)°. The DFT-calculated value is 172°, clearly showing that this is not a packing but an electronic effect.

EXPERIMENTAL SECTION

All manipulations were performed under an inert atmosphere of argon by using Schlenk techniques or in a MBraun inert-gas glovebox. The solvents were purified according to standard procedures.[28] The deuterated solvents were purchased from Aldrich and dried over 4 Å molecular sieves. [$NiCl_2$(DME)][29] and potassium graphite (KC_8)[30] were prepared according to the literature. ^{1}H, ^{13}C{^{1}H}, and ^{31}P{^{1}H} NMR spectra were recorded on Bruker AVANCE-250 and AVANCE-300 DPX spectrometers. ^{1}H and ^{13}C{^{1}H} NMR spectra were referenced internally to residual protio-solvent and solvent resonances, respectively, and are reported relative to tetramethylsilane (δ = 0 ppm). ^{31}P{^{1}H} NMR spectra were referenced externally to H_3PO_4 (85%) (δ = 0 ppm).

Magnetization measurements as a function of temperature were performed on powder samples using a SQUID magnetometer (Quantum Design MPMS). The curves were obtained at 0.1 T for temperatures ranging from 5 to 300 K. The susceptibility values were corrected for diamagnetism of the constituent atoms using Pascal constants.

All mass spectrometric measurements were performed on an Esquire 3000^{plus} 3D-quadrupole ion trap mass spectrometer (Bruker Daltonics, Bremen, Germany) in positive ion mode electrospray ionization (ESI-MS). Mass calibration was done with a commercial mixture of perfluorinated trialkyl-triazines (ES Tuning Mix, Agilent Technologies, Santa Clara, CA, USA). All analytes were dissolved in MeOH "Lichrosolv" quality (Merck, Darmstadt, Germany) to a concentration of roughly 1 mg/mL. Direct infusion experiments were carried out using a Cole Parmer model 74900 syringe pump (Cole Parmer Instruments, Vernon Hills, IL, USA) at a flow rate of 2 μL/min. Full-scan MS scans were measured in the range m/z 100−1000 with the target mass set to m/z 800. Further experimental conditions include drying gas temperature, 150 °C; capillary voltage, −4 kV; skimmer voltage, 40 V; octapole and lens voltages, according to the target mass set. Helium was used as buffer gas for full scans. All mass calculations are based on the lowest mass cobalt and nickel isotopes (^{59}Co and ^{58}Ni isotope). Mass spectra were averaged during a data acquisition time of 1 to 2 min, and one analytical scan consisted of five successive microscans, resulting in 50 and 100 analytical scans, respectively, for the final mass spectrum.

***N,N′*-Bis(di-isopropylphosphino)-*N,N′*-dimethyl-1,3-diaminobenzene (PCP^{Me}-*i*Pr) (1).** A suspension of *N,N′*-dimethyl-1,3-benzenediamine (4.9 g, 36.1 mmol) in THF (250 mL) was cooled to −78 °C, and *n*BuLi (73.98 mmol, 29.6 mL of a 2.5 M solution in hexane) was added in a dropwise fashion. The mixture was allowed to reach room temperature and stirred for an additional 3 h. Upon cooling to 0 °C, P*i*Pr$_2$Cl (72.18 mmol, 10.97 mL) was added slowly via a syringe and the reaction mixture was allowed to reach room temperature and stirred for 20 h. After that, the solvent was removed under reduced pressure and the crude product was dissolved in toluene (150 mL) and stirred well at 60 °C for 20 min. A precipitate of lithium chloride was removed by filtration, the solvent was evaporated, and the oily residue was dried under vacuum. Colorless crystals of the pure product were obtained from a saturated acetonitrile solution after cooling to −30 °C for 24 h. Yield: 12.5 g (94%). Anal. Calcd for $C_{20}H_{38}N_2P_2$ (368.49): C, 65.19; H, 10.39; N, 7.60. Found: C, 65.01; H, 10.45; N, 7.68. ^{1}H NMR (δ, $CDCl_3$, 20 °C): 7.09 (t, $^3J_{HH}$= 2.5 Hz, 1H, Ph), 7.06 (d, $^4J_{HP}$ = 7.5 Hz, 1H, Ph), 6.71 (dt, $^3J_{HH}$ = 2.4 Hz, $^4J_{HP}$ = 8.2 Hz, 2H, Ph), 2.97 (d, $^3J_{HP}$ = 1.5 Hz, 6H, NCH_3), 2.01−2.13 (m, 4H, C*H*), 1.00−1.17 (m, 24H, CH_3). ^{13}C{^{1}H} NMR (δ, $CDCl_3$, 20 °C): 153.2 (d, $^2J_{CP}$ = 19.5 Hz, Ph), 128.1 (py), 107.4 (d, $^3J_{CP}$ = 16.6 Hz, Ph), 105.3 (vt, $^4J_{CP}$ = 16.1 Hz, Ph), 34.6 (d, $^2J_{CP}$ = 7.5 Hz, NCH_3), 26.6 (d, $^1J_{CP}$ = 16.0 Hz, CH), 19.4 (m, CH_3). ^{31}P{^{1}H} NMR (δ, $CDCl_3$, 20 °C): 71.1.

[Co(PCP^{Me}-*i*Pr)Cl] (2). A suspension of **1** (1.0 g, 2.72 mmol) in THF (10 mL) was cooled to −78 °C, and *n*-BuLi (2.86 mmol, 1.14 mL of a 2.5 M solution in *n*-hexane) was slowly added in a dropwise fashion. The mixture was then allowed to reach room temperature and stirred for 2 h. After that, 1.1 equiv of anhydrous $CoCl_2$ (390 mg, 2.99 mmol) was added, whereupon the solution rapidly turned deep red. After the mixture was stirred for 24 h, the solvent was removed under vacuum. The resulting crude product was redissolved in CH_2Cl_2, insoluble materials were removed by filtration, and the solvent was evaporated under vacuum to afford the product as a red solid. Yield: 1.2 g (96%). Anal. Calcd for $C_{20}H_{37}ClCoN_2P_2$ (461.86): C, 52.01; H, 8.08; N, 6.07. Found: C, 52.15; H, 8.14; N, 6.15. μ_{eff} = 2.3(1) μ_B.

[Ni(PCP^{Me}-*i*Pr)Cl] (3). This complex was prepared in analogous fashion to **2** with $NiCl_2$(DME) (327 mg, 1.50 mmol), **1** (500 mg, 1.36 mmol), and *n*BuLi (1.43 mmol, 571 μL of a 2.5 M solution in *n*-hexane). Yield: 97% (610 mg). Anal. Calcd for $C_{20}H_{37}ClN_2NiP_2$ (461.62): C, 52.04; H, 8.08; N, 6.07. Found: C, 51.91; H, 8.13; N, 6.13. ^{1}H NMR (δ, CD_2Cl_2, 20 °C): 6.91 (t, $^3J_{HH}$= 8.4 Hz,1H, Ph), 5.86 (d, $^3J_{HH}$ = 7.9 Hz, 2H, Ph), 2.87 (vt, $^3J_{HP}$ = 2.5 Hz, 6H, NCH_3), 2.46−2.60 (m, 4H, C*H*), 1.37−1.46 (dd, $^3J_{HH}$ = 7.5 Hz, $^3J_{HP}$ = 15 Hz, 12H, CH_3), 1.25−1.33 (dd, $^3J_{HH}$ = 7.5 Hz, $^3J_{HP}$ = 15 Hz, 12H, CH_3). ^{13}C{^{1}H} NMR (δ, CD_2Cl_2, 20 °C): 161.6 (t, $^2J_{CP}$= 16.8 Hz, Ph), 126.9 (Ph), 120.9 (vt, $^2J_{CP}$= 19.8 Hz, Ph), 100.4 (vt, $^3J_{CP}$= 5.9 Hz, Ph), 31.9 (s, NMe), 25.4 (t, $^1J_{CP}$= 11.1 Hz, CH), 17.8 (CH_3). ^{31}P{^{1}H} NMR (δ,CD_2Cl_2, 20 °C): 120.4.

[Co(PCP^{Me}-*i*Pr)(CO)Cl] (4). A suspension of **2** (200 mg, 0.43 mmol) in toluene was stirred in a CO atmosphere, and the solution immediately turned from red to brown. After removal of the solvent under vacuum complex **4** was obtained as a brown solid. Yield: 94% (200 mg). Anal. Calcd for $C_{21}H_{37}ClCoN_2OP_2$ (489.87): C, 51.49; H, 7.61; N, 5.72. Found: C, 51.65; H, 7.69; N, 5.65. μ_{eff} = 2.0(1) μ_B. IR (ATR, cm^{-1}): 1948 (ν_{CO}).

[Co(PCP^{Me}-*i*Pr)(py)Cl] (5). To a suspension of **2** (200 mg, 0.43 mmol) in toluene (5 mL) was added excess pyridine (0.5 mL), and the mixture was stirred for 2 h. After removal of the solvent under reduced pressure, complex **5** was obtained in analytically pure form as a yellow solid. Yield: 222 mg (95%). Anal. Calcd for $C_{25}H_{42}ClCoN_3P_2$ (540.96): C, 55.51; H, 7.83; N, 7.77. Found: C, 55.66; H, 7.79; N, 7.82. μ_{eff} = 2.4(1) μ_B.

[Co(PCP^{Me}-*i*Pr)(CO)$_2$]SbF$_6$ (6). A suspension of **2** (100 mg, 0.216 mmol) in CH_2Cl_2 was treated with $AgSbF_6$ (75 mg, 0.217 mmol) under a CO atmosphere, and the mixture was stirred for 1 h. After that, the solution was filtered through Celite, and the solvent was removed under reduced pressure to afford a blue-green solid. Yield: 147 mg (93%). Anal. Calcd for $C_{22}H_{37}CoF_6N_2O_2P_2Sb$ (717.18): C, 36.79; H, 5.19; N, 3.90. Found: C, 36.85; H, 5.23; N, 3.88. IR (ATR, cm^{-1}): 2013 (ν_{CO}), 2046 (ν_{CO}). μ_{eff} = 1.9(1)μ_B. ESI-MS (m/z, CH_3CN) positive ion: 454.2 [M − CO]$^+$.

[Co(PCP^{Me}-*i*Pr)Cl$_2$] (7). A suspension of **2** (200 mg, 0.43 mmol) in THF was reacted with $CuCl_2$ (64 mg, 0.47 mmol), and the mixture was stirred for 30 min. After that, the solvent was evaporated, CH_2Cl_2 was added, and the mixture was stirred for 15 min. After that, the solution was filtered through Celite, and the solvent was removed under reduced pressure to afford a green solid. Yield: 93% (200 mg). Anal. Calcd for $C_{20}H_{37}Cl_2CoN_2P_2$ (497.31): C, 48.30; H, 7.50; N, 5.63. Found: C, 48.35; H, 7.49; N, 5.67. ^{1}H NMR (δ, C_6D_6, 20 °C): 37.22 (br, 1H), 29.63 (br, 2H), 3.63 (br, 6H), 0.31−2.35 (br, 22H), −6.37 (br, 6H). μ_{eff} = 3.1 μ_B (CH_2Cl_2, Evans method).

[Co(PCP^{Me}-*i*Pr)(CO)$_2$] (8). A suspension of **2** (100 mg, 0.23 mmol) in toluene was treated with 1.1 equiv of freshly prepared KC_8 under a CO atmosphere, and the mixture was stirred for 30 min. After that, the product was filtered through Celite, the solvent was removed under vacuum, and an analytically pure yellow solid was obtained. Yield: 90% (100 mg). Anal. Calcd for $C_{22}H_{37}CoN_2O_2P_2$ (482.43): C, 54.77; H, 7.73; N, 5.81. Found: C, 54.75; H, 7.79; N, 5.72. ^{1}H NMR (δ, C_6D_6, 20 °C): 7.19 (t, $^3J_{HH}$ = 9.2 Hz, 1H, Ph), 6.17 (d, $^3J_{HH}$ = 7.5 Hz, 2H, Ph), 2.61 (s, 6H, NCH_3), 2.11−2.26 (m, 4H, C*H*), 1.27 (dd, $^3J_{HH}$ = 7.5 Hz, $^3J_{HP}$ = 17.5 Hz, 12H, CH_3), 1.09 (dd, $^3J_{HH}$ = 7.5 Hz, $^3J_{HP}$ = 12.5 Hz, 12H, CH_3). ^{13}C{^{1}H} NMR (δ, C_6D_6, 20 °C): 207.6 (br, CO), 157.3 (t, $^4J_{CP}$ = 15.0 Hz, Ph), 129.0 (Ph), 124.3 (Ph), 100.6 (vt,

dx.doi.org/10.1021/om5007769 | *Organometallics* 2014, 33, 6132−6140

$^3J_{CP}$ = 5.9 Hz, Ph), 31.9 (NCH_3), 31.4 (vt, $^1J_{CP}$ = 11.8 Hz, *C*H), 18.2 (d, $^2J_{CP}$ = 10.6 Hz, CH_3), the C_{ipso} carbon atom was not detected. $^{31}P\{^1H\}$ NMR (δ, C_6D_6, 20 °C): 170.6. IR (ATR, cm^{-1}): 1906 (ν_{CO}), 1963 (ν_{CO}).

[Co(PCP^{Me}-*i*Pr)(CH_3CN)$_3$](SbF_6)$_2$ (9). A suspension of **8** (200 mg, 0.43 mmol) in CH_3CN (5 mL) was treated with $AgSbF_6$ (274 mg, 0.80 mmol), and the mixture was stirred for 30 min. After that, the solvent was evaporated and the crude product redissolved in CH_2Cl_2. Insoluble materials were removed by filtration, and upon removal of the solvent a brown solid was obtained. Yield: 265 mg (93%). Anal. Calcd for $C_{26}H_{46}CoF_{12}N_5P_2Sb_2$ (1021.07): C, 30.58; H, 4.54; N, 6.86. Found: C, 30.65; H, 4.69; N, 6.52. ^1H NMR (δ, CD_2Cl_2, 20 °C): 7.18 (t, $^3J_{HH}$ = 15.0 Hz, 1H, Ph), 6.29 (d, $^3J_{HH}$ = 10.0 *Hz*, 1H, Ph), 3.18 (s, 6H, NCH_3), 2.90−3.07 (m, 4H, *C*H), 2.59 (s, 3H, CH_3CN), 2.27 (s, 6H, CH_3CN), 1.38−1.51 (m, 24H, CH_3). $^{13}C\{^1H\}$ NMR (δ, CD_2Cl_2, 20 °C): 158.2 (t, $^2J_{CP}$ = 11.6 Hz, Ph), 135.3 (*C*N), 131.5 (*C*N), 129.0 (Ph), 111.5 (d, $^2J_{CP}$ = 5.6 Hz, Ph), 104.8 (d, $^3J_{CP}$ = 3.9 Hz, Ph), 34.1 (NCH_3), 28.4 (*C*H), 18.7 (CH_3), 17.8 (CH_3), 5.4 (CH_3CN), 3.4 (CH_3CN). $^{31}P\{^1H\}$ NMR (δ, CD_2Cl_2, 20 °C): 133.2.

[Ni(PCP^{Me}-*i*Pr)(CO)]SbF_6 (10). A suspension of **3** (100 mg, 0.217 mmol) in CH_2Cl_2 was treated with $AgSbF_6$ (89 mg, 0.26 mmol) under a CO atmosphere, and the mixture was stirred for 2 h. After that, the solution was filtered through Celite, and the solvent was removed under reduced pressure to afford a yellow solid. Yield: 130 mg (87%). Anal. Calcd for $C_{21}H_{37}NiF_6N_2OP_2Sb$ (689.93): C, 36.56; H, 5.41; N, 4.06. Found: C, 36.45; H, 5.40; N, 3.96. ^1H NMR (δ, CD_2Cl_2, 20 °C): 7.21 (t, $^3J_{HH}$ = 8.7 Hz, 1H, Ph), 6.18 (d, $^3J_{HH}$ = 8.4, 2H, Ph), 2.81 (vt, $^3J_{HP}$ = 2.5 Hz, 6H, NCH_3), 2.69−2.85 (m, 4H, *C*H), 1.24−1.43 (m, 24H, CH_3). $^{13}C\{^1H\}$ NMR (δ, CD_2Cl_2, 20 °C): 189.9 (t, $^2J_{CP}$ = 13.7 Hz, CO), 161.9 (t, $^2J_{CP}$ = 14.0 Hz, Ph), 133.0 (s, Ph), 102.7 (t, $^2J_{CP}$ = 6.6 Hz, ^{4}Ph), 32.4 (NCH_3), 28.1 (vt, $^1J_{CP}$ = 14.0 Hz, *C*H), 18.5 (CH_3), 18.0 (s, CH_3), the C_{ipso} carbon atom was not detected. $^{31}P\{^1H\}$ NMR (δ, CD_2Cl_2, 20 °C): 148.6. IR (ATR, cm^{-1}): 2051 (ν_{CO}). ESI-MS (*m*/*z*, CH_3CN) positive ion: 453.2 $[M]^+$, 425.2 $[M - CO]^+$.

X-ray Structure Determination. X-ray diffraction data for **2**, **3**, **4**, **5**, **6**, **7**, and **10** were collected at *T* = 100 K on a Bruker Kappa APEX-2 CCD diffractometer with an Oxford Cryosystems cooler using graphite-monochromatized Mo Kα radiation (λ = 0.710 73 Å). For **8** a Bruker SMART APEX three-circle diffractometer was used instead. Redundant data sets were collected in φ- and ω-scan modes (**8**: only ω-scans) covering the whole reciprocal sphere. Automatic lattice parameter determination failed for **2**. Inspection of the reflection data revealed the existence of two domains, which were separated using the RLATT tool of the Apex2 software suite.[31] The reflections of both domains could be assigned to two isometric monoclinic cells, related by a reflection at (100). Data of all crystals were reduced to intensity values with SAINT, and an absorption correction was applied with the multiscan approach implemented in SADABS (**2**: TWINABS).[30] The structures were solved by charge flipping using SUPERFLIP[32] and refined against *F* with JANA2006.[33] Non-hydrogen atoms were refined with anisotropic displacement parameters. Hydrogen atoms were placed at calculated positions and refined as riding on the parent C atom. Since **2** crystallizes in the non-centrosymmetric space group *Pc*, it was refined as four domains with the twin-volume fractions of three domains as refinable parameter. The crystal was composed of two domains related by reflection at (100), whereas contributions of the inverted domains are negligible (Flack parameter 0.038(6)). In **5** significant albeit smeared out electron density was observed in channels of the structure around the 3-fold rotoinversion axes. Attempts to model disordered pentane solvent molecules were unsuccessful, and therefore the contribution of this electron cloud (65*e* per channel and unit cell, slightly less than one pentane molecule, 72*e*) to the intensity data was removed using the SQUEEZE routine of PLATON.[34] Molecular graphics were generated with the program MERCURY.[35] Crystal data and experimental details are given in Tables S1 and S2 (Supporting Information).

Computational Details. All calculations were performed using the GAUSSIAN 09 software package[36] on the Phoenix Linux Cluster of the Vienna University of Technology. The optimized geometries were obtained with spin-unrestricted calculations, using the B3LYP functional.[37] That functional includes a mixture of Hartree−Fock[38] exchange with DFT[21] exchange−correlation, given by Becke's three-parameter functional with the Lee, Yang, and Parr correlation functional, which includes both local and nonlocal terms.

The basis set used for the geometry optimizations (basis b1) consisted of the Stuttgart/Dresden ECP (SDD) basis set[39] to describe the electrons of Co and Ni and a standard 6-31G(d,p) basis set[40] for all other atoms. Frequency calculations were performed to confirm the nature of the stationary points, yielding no imaginary frequency for the minima. The electronic energies (E_{b1}) obtained at the B3LYP/b1 level of theory were converted to free energy at 298.15 K and 1 atm (G_{b1}) by using zero-point energy and thermal energy corrections based on structural and vibration frequency data calculated at the same level. The molecular orbitals presented in Figure 6a resulted from single point restricted open-shell calculations performed on the optimized structures.

Single-point energy calculations were performed using the M06 functional and a standard 6-311++G(d,p) basis set,[41] on the geometries optimized at the B3LYP/b1 level. The M06 functional is a hybrid meta-GGA functional developed by Truhlar and Zhao,[42] and it was shown to perform very well for transition metal systems, providing a good description of weak and long-range interactions.[43] Solvent effects (benzene) were considered in the M06/6-311++G(d,p)//B3LYP/b1 energy calculations using the polarizable continuum model (PCM) initially devised by Tomasi and co-workers[44] with radii and nonelectrostatic terms of the SMD solvation model, developed by Truhler et al.[45]

The free energy values presented in the text (G_{b2}^{soln}) were derived from the electronic energy values obtained at the M06/6-311++G(d,p)//B3LYP/b1 level, including solvent effects (E_{b2}^{soln}), according to the following expression: $G_{b2}^{soln} = E_{b2}^{soln} + G_{b1} - E_{b1}$. Three-dimensional representations of the orbitals were obtained with the program Chemcraft.[46]

■ ASSOCIATED CONTENT

Ⓢ Supporting Information

Complete crystallographic data, ^1H, $^{13}C\{^1H\}$, and $^{31}P\{^1H\}$ NMR spectra of all diamagnetic complexes, ^1H NMR spectrum of complex **7**, as well as technical details in CIF format for **2**, **3**, **4**, **5**, **6**, **8**, and **10**. This material is available free of charge via the Internet at http://pubs.acs.org.

■ AUTHOR INFORMATION

Corresponding Author

*E-mail: kkirch@mail.tuwien.ac.at.

Notes

The authors declare no competing financial interest.

■ ACKNOWLEDGMENTS

Financial support by the Austrian Science Fund (FWF) is gratefully acknowledged (Project No. P24583-N28), and L.F.V. and L.P.F. acknowledge Fundação para a Ciência e Tecnologia, Projecto Estratégico, PEst-OE/QUI/UI0100/2013 and PEst-OE/FIS/UI0261/2014, respectively. The X-ray center of the Vienna University of Technology is acknowledged for financial support and for providing access to the single-crystal diffractometer.

■ REFERENCES

(1) For reviews on pincer complexes, see: (a) Albrecht, M.; van Koten, G. *Angew. Chem., Int. Ed.* **2001**, *40*, 3750−3781. (b) van der Boom, M. E.; Milstein, D. *Chem. Rev.* **2003**, *103*, 1759−1792. (c) Singleton, J. T. *Tetrahedron* **2003**, *59*, 1837. (d) Bhattacharya, P.; Guan, H. *Comment Inorg. Chem.* **2011**, *32*, 88. (e) Schneider, S.; Meiners, J.; Askevold, B. *Eur. J. Inorg. Chem.* **2012**, 412−429. (f) Morales-Morales, D.; Jensen, C. M., Eds. *The Chemistry of Pincer*

Compounds; Elsevier: Amsterdam, 2007. (g) van Koten, G., Milstein, D., Eds.; *Organometallic Pincer Chemistry*; Topics in Organometallic Chemistry Vol. *40*; Springer: Berlin, 2013.
(2) Benito-Garagorri, D.; Kirchner, K. *Acc. Chem. Res.* **2008**, *41*, 201−213.
(3) Benito-Garagorri, D.; Bocokić, V.; Mereiter, K.; Kirchner, K. *Organometallics* **2006**, *25*, 3817−3823.
(4) For recent examples of Fe PNP complexes based on the 2,6-diaminopyridine scaffold see: (a) Bichler, B.; Holzhacker, C.; Stöger, B.; Puchberger, M.; Veiros, L. F.; Kirchner, K. *Organometallics* **2013**, *32*, 4114−4121. (b) Benito-Garagorri, D.; Alves, L. G.; Veiros, L. F.; Standfest-Hauser, C. M.; Tanaka, S.; Mereiter, K.; Kirchner, K. *Organometallics* **2010**, *29*, 4932−4942. (c) Benito-Garagorri, D.; Puchberger, M.; Mereiter, K.; Kirchner, K. *Angew. Chem., Int. Ed.* **2008**, *47*, 9142−9145.
(5) For recent examples of Mo PNP complexes based on the 2,6-diaminopyridine scaffold see: (a) Öztopcu, Ö.; Holzhacker, C.; Puchberger, M.; Weil, M.; Mereiter, K.; Veiros, L. F.; Kirchner, K. *Organometallics* **2013**, *32*, 3042−3052. (b) de Aguiar, S. R. M. M.; Stöger, B.; Pittenauer, E.; Allmaier, G.; Puchberger, M.; Veiros, L. F.; Kirchner, K. *J. Organomet. Chem.* **2014**, *760*, 74−83.
(6) Xu, G. Q.; Sun, H. J.; Li, X. Y. *Organometallics* **2009**, *28*, 6090−6095.
(7) Lian, Z.; Xu, G.; Li, X. *Acta Crystallogr., Sect. E: Struct. Rep. Online* **2010**, *E66*, m636.
(8) Hebden, T. J.; St. John, A. J.; Gusev, D. G.; Kaminsky, W.; Goldberg, K. I.; Heinekey, D. M. *Angew. Chem., Int. Ed.* **2011**, *50*, 1873−1876.
(9) Zhu, G.; Li, X.; Xu, G.; Wang, L.; Sun, H. *Dalton Trans.* **2014**, *43*, 8595−8598.
(10) Kent, M. A.; Woodall, C. H.; Haddow, M. F.; McMullin, C. L.; Pringle, P. G.; Wass, D. F. *Organometallics* **2014**, in press.
(11) Fryzuk, M. D.; Leznoff, D. B.; Thompson, R. C.; Rettig, S. J. *J. Am. Chem. Soc.* **1998**, *120*, 10126−10135.
(12) (a) Ingleson, M. J.; Pink, M.; Caulton, K. G. *J. Am. Chem. Soc.* **2006**, *128*, 4248−4249. (b) Ingleson, M.; Fan, H.; Pink, M.; Tomaszewski, J.; Caulton, K. G. *J. Am. Chem. Soc.* **2006**, *128*, 1804−1805. (c) Ingleson, M. J.; Fullmer, B. C.; Buschhorn, D. T.; Fan, H.; Pink, M.; Huffman, J. C.; Caulton, K. G. *Inorg. Chem.* **2008**, *47*, 407−409. (d) Ingleson, M. J.; Pink, M.; Fan, H.; Caulton, K. G. *J. Am. Chem. Soc.* **2008**, *130*, 4262−4276. (e) Ingleson, M. J.; Pink, M.; Fan, H.; Caulton, K. G. *Inorg. Chem.* **2007**, *46*, 10321−10334.
(13) (a) Rozenel, S. S.; Padilla, R.; Arnold, J. *Inorg. Chem.* **2013**, *52*, 11544−11550. (b) Rozenel, S. S.; Padilla, R.; Camp, C.; Arnold, J. *Chem. Commun.* **2014**, *50*, 2612−2614.
(14) Fout, A. R.; Basuli, F.; Fan, H.; Tomaszewski, J.; Huffman, J. C.; Baik, M.-H.; Mindiola, D. J. *Angew. Chem., Int. Ed.* **2006**, *45*, 3291−3295.
(15) Semproni, S. P.; Milsmann, C.; Chirik, P. J. *J. Am. Chem. Soc.* **2014**, *136*, 9211−9224.
(16) Khaskin, E.; Diskin-Posner, Y.; Weiner; Leitus, L. G.; Milstein, D. *Chem. Commun.* **2013**, *49*, 2771−2773.
(17) Wu, S.; Li, X.; Xiong, Z.; Xu, W.; Lu, Y.; Sun, H. *Organometallics* **2013**, *32*, 2327−2337.
(18) Hosokawa, S.; Ito, J.; Nishiyama, H. *Organometallics* **2013**, *32*, 3980−3985.
(19) Sauer, D. C.; Kruck, M.; Wadepohl, H.; Enders, M.; Gade, L. H. *Organometallics* **2013**, *32*, 885−892.
(20) (a) Carlin, R. L. *Magnetochemistry*; Springer-Verlag: Heidelberg, 1986. (b) Orchard, A. F. *Magnetochemistry*; Oxford University Press, 2003.
(21) Parr, R. G.; Yang, W. *Density Functional Theory of Atoms and Molecules*; Oxford University Press: New York, 1989.
(22) Obtained at the B3LYP/b1 level (see Computational Details).
(23) For a discussion and references of bent CO ligands, see: Pelczar, E. M.; Emge, T. J.; Krogh-Jespersen, K.; Goldman, A. S. *Organometallics* **2008**, *27*, 5759−5767.
(24) Hoffmann, R.; Chen, M. M. L.; Elian, M.; Rossi, A. R.; Mingos, D. M. P. *Inorg. Chem.* **1974**, *13*, 2666−2675.
(25) Falvello, L.; Gerloch, M. *Acta Crystallogr. B* **1979**, *B35*, 2547.
(26) Sur, S. K. *J. Magn. Reson.* **1989**, *82*, 169.
(27) Free energy values including solvent effects (PCM model; see Computational Details).
(28) Perrin, D. D.; Armarego, W. L. F. *Purification of Laboratory Chemicals*, 3rd ed.; Pergamon: New York, 1988.
(29) Kermagoret, A.; Braunstein, P. *Organometallics* **2008**, *27*, 88−99.
(30) Weitr, I. S.; Rabinovitz, M. *J. Chem. Soc., Perkin Trans. 1* **1993**, *1*, 117−120.
(31) Bruker computer programs: *APEX2*, *SAINT*, *SADABS*, and *TWINABS*; Bruker AXS Inc.: Madison, WI, 2012.
(32) Palatinus, L.; Chapuis, G. *J. Appl. Crystallogr.* **2007**, *40*, 786−790.
(33) Petříček, V.; Dušek, M.; Palatinus, L. *Z. Kristallogr.* **2014**, *229*, 345−352.
(34) Spek, A. L. *J. Appl. Crystallogr.* **2003**, *36*, 7−3.
(35) Macrae, C. F.; Edgington, P. R.; McCabe, P.; Pidcock, E.; Shields, G. P.; Taylor, R.; Towler, M.; van de Streek, J. *J. Appl. Crystallogr.* **2006**, *39*, 453−457.
(36) Frisch, M. J.; et al. *Gaussian 09*, Revision A.02; Gaussian, Inc.: Wallingford, CT, 2009.
(37) (a) Becke, A. D. *J. Chem. Phys.* **1993**, *98*, 5648−5652. (b) Miehlich, B.; Savin, A.; Stoll, H.; Preuss, H. *Chem. Phys. Lett.* **1989**, *157*, 200−206. (c) Lee, C.; Yang, W.; Parr, G. *Phys. Rev. B* **1988**, *37*, 785−789.
(38) Hehre, W. J.; Radom, L.; Schleyer, P. v. R.; Pople, J. A. *Ab Initio Molecular Orbital Theory*; John Wiley & Sons: New York, 1986.
(39) (a) Haeusermann, U.; Dolg, M.; Stoll, H.; Preuss, H. *Mol. Phys.* **1993**, *78*, 1211−1224. (b) Kuechle, W.; Dolg, M.; Stoll, H.; Preuss, H. *J. Chem. Phys.* **1994**, *100*, 7535−7542. (c) Leininger, T.; Nicklass, A.; Stoll, H.; Dolg, M.; Schwerdtfeger, P. *J. Chem. Phys.* **1996**, *105*, 1052−1059.
(40) (a) McLean, A. D.; Chandler, G. S. *J. Chem. Phys.* **1980**, *72*, 5639−5648. (b) Krishnan, R.; Binkley, J. S.; Seeger, R.; Pople, J. A. *J. Chem. Phys.* **1980**, *72*, 650−654. (c) Wachters, A. J. H. *J. Chem. Phys.* **1970**, *52*, 1033−1036. (d) Hay, P. J. *J. Chem. Phys.* **1977**, *66*, 4377−4384. (e) Raghavachari, K.; Trucks, G. W. *J. Chem. Phys.* **1989**, *91*, 1062−1065. (f) Binning, R. C., Jr.; Curtiss, L. A. *J. Comput. Chem.* **1990**, *11*, 1206. (g) McGrath, M. P.; Radom, L. *J. Chem. Phys.* **1991**, *94*, 511−516.
(41) (a) McClean, A. D.; Chandler, G. S. *J. Chem. Phys.* **1980**, *72*, 5639−5648. (b) Krishnan, R.; Binkley, J. S.; Seeger, R.; Pople, J. A. *J. Chem. Phys.* **1980**, *72*, 650−654. (c) Wachters, A. J. H. *J. Chem. Phys.* **1970**, *52*, 1033−1036. (d) Hay, P. J. *J. Chem. Phys.* **1977**, *66*, 4377−4384. (e) Raghavachari, K.; Trucks, G. W. *J. Chem. Phys.* **1989**, *91*, 1062−1065. (f) Binning, R. C., Jr.; Curtiss, L. A. *J. Comput. Chem.* **1990**, *11*, 1206−1216. (g) McGrath, M. P.; Radom, L. *J. Chem. Phys.* **1991**, *94*, 511−516. (h) Clark, T.; Chandrasekhar, J.; Spitznagel, G. W.; Schleyer, P. v. R. *J. Comput. Chem.* **1983**, *4*, 294−301. (i) Frisch, M. J.; Pople, J. A.; Binkley, J. S. *J. Chem. Phys.* **1984**, *80*, 3265−3269.
(42) Zhao, Y.; Truhlar, D. G. *Theor. Chem. Acc.* **2008**, *120*, 215−241.
(43) (a) Zhao, Y.; Truhlar, D. G. *Acc. Chem. Res.* **2008**, *41*, 157−167. (b) Zhao, Y.; Truhlar, D. G. *Chem. Phys. Lett.* **2011**, *502*, 1−13.
(44) (a) Cancès, M. T.; Mennucci, B.; Tomasi, J. *J. Chem. Phys.* **1997**, *107*, 3032−3041. (b) Cossi, M.; Barone, V.; Mennucci, B.; Tomasi, J. *Chem. Phys. Lett.* **1998**, *286*, 253−260. (c) Mennucci, B.; Tomasi, J. *J. Chem. Phys.* **1997**, *106*, 5151−5158. (d) Tomasi, J.; Mennucci, B.; Cammi, R. *Chem. Rev.* **2005**, *105*, 2999−3094.
(45) Marenich, A. V.; Cramer, C. J.; Truhlar, D. G. *J. Phys. Chem. B* **2009**, *113*, 6378−6396.
(46) http://www.chemcraftprog.com/.